Observation of zone folding induced acoustic topological insulators and the role of spin-mixing defects

Yuanchen Deng,[1] Hao Ge,[2] Yuan Tian,[2] Minghui Lu,[2,*] and Yun Jing[1,†]

[1]*Department of Mechanical and Aerospace Engineering, North Carolina State University, Raleigh, North Carolina 27695, USA*

[2]*National Laboratory of Solid State Microstructures and Department of Materials Science and Engineering, Nanjing University, Nanjing, Jiangsu 210093, China*

(Received 1 May 2017; published 27 November 2017)

This article reports on the experimental realization of a flow-free, pseudospin-based acoustic topological insulator designed using the strategy of zone folding. Robust sound one-way propagation is demonstrated with the presence of non-spin-mixing defects. On the other hand, it is shown that spin-mixing defects, which break the geometric symmetry and therefore the pseudo-time-reversal symmetry, can open up nontrivial band gaps within the edge state frequency band, and their width can be tailored by the extent of the defect. This provides a possible route for realizing tunable acoustic topological insulators.

DOI: 10.1103/PhysRevB.96.184305

I. INTRODUCTION

Recent discoveries in condensed matter physics have opened possibilities for topological physics which are characterized by either the quantum Hall effect (QHE) [1,2] or quantum spin Hall effect (QSHE) [3,4]. Translating the concept of topological phases [5] to classical waves, such as optic [6–12], acoustic [13–27], and elastic waves [28–32], is currently an active area of research. There are several barriers in realizing topological states in acoustics, such as the absence of polarization in longitudinal waves and the difficulty of breaking the time-reversal symmetry in Hermitian systems. For acoustic topological Chern insulators, external fields such as circulating fluids have been used to break the time-reversal symmetry [17–20]. The inevitable dynamic instability and flow-induced noise, however, could pose great challenges for practical applications. On the other hand, the intrinsic spin-1/2 fermionic characteristic is the underpinning component of the QSHE for electrons. Direct analogy in acoustics is nontrivial, though, due to the spin-0 nature of acoustic waves. To address this issue, He *et al.* [25] and Mei *et al.* [33] independently provided a pseudospin approach for designing flow-free acoustic topological insulators based on accidentally formed double Dirac cones in a phononic crystal [34,35]. However, the double Dirac cone can only be obtained at a fixed filling ratio, which is typically found by a trial-and-error approach. In photonic crystals, the "zone folding" mechanism was proposed to form double Dirac cones [9] without relying on a fixed filling ratio. By expanding the unit cell of the lattice, the Brillouin zone will fold and the high symmetry points K and K' in the original Brillouin zone are mapped to the Γ point of the new Brillouin zone, giving rise to double Dirac cones. A similar concept was introduced to acoustics to construct double Dirac cones as well as acoustic topological insulators for robust one-way propagation [24]. An experimental demonstration, however, was not provided. In addition, previous research has only focused on non-spin-mixing defects (the ones that do not affect the pseudospin states) [25] in phononic topological insulators. Spin-mixing defects, on the other hand, are largely unexplored.

In this article, we provide experimental evidence of robust one-way propagation of sound in phononic crystal-based topological insulators designed using zone folding. Furthermore, spin-mixing defects are investigated and their nontrivial roles in tailoring the edge states are numerically and experimentally observed. Spin-mixing defects have yet to be studied in detail in phononic or photonic topological insulators, although their nontrivial roles have been noted in the past [9,25,27,36].

II. DESIGN

In a traditional triangular lattice phononic crystal featuring a lattice constant a_0, the unit cell could be chosen as a hexagon possessing a single "atom" at the center [Figs. 1(a) and 1(b)]. The unit cell has a sixfold rotational symmetry C_{6v} as well as a translational symmetry T_{a_0} corresponding to the lattice constant a_0. Therefore, the band structure for the unit cell has single Dirac cones at the high symmetry points K and K' [K' is not shown in Fig. 2(a) due to the symmetry]. Here, we modify the unit cells so that the physical domain is expanded by a factor of $\sqrt{3}$, yielding a lattice constant $a = \sqrt{3}a_0$. While the original "atom" remains at the center, there are six other "1/3 atoms" at each corner of the hexagon, which naturally also alters the Brillouin zone. As the size of the unit cell is expanded by $\sqrt{3}$, the size of the Brillouin zone consequently is reduced by the same factor. Additionally, there is a $\pi/3$ rotation from the original orientation and the change of the Brillouin zone will map the single Dirac cones from K and K' to the new Brillouin zone at the Γ point, forming double Dirac cones [Figs. 1(c) and 2(b)]. In our design for simulations and experiments, the new lattice constant a is 10 mm. The radius of the atom r is $0.35a$, i.e., 3.5 mm. Note that the existence of double Dirac cones in the expanded unit cell does not depend upon a fixed filling ratio because of the zone folding mechanism (Appendix A). The new unit cell has double Dirac cones at $f_0 = 17800$ Hz, as shown by the band structure in Fig. 2(b). Since the C_{6v} symmetry is still preserved in the expanded unit cell, there are also single Dirac cones at K and K' of the new Brillouin zone. The purpose of introducing the double Dirac cones is to gain a fourfold degeneracy, which is the key component to form artificial pseudospin-1/2 states.

*luminghui@nju.edu.cn

†yjing2@ncsu.edu

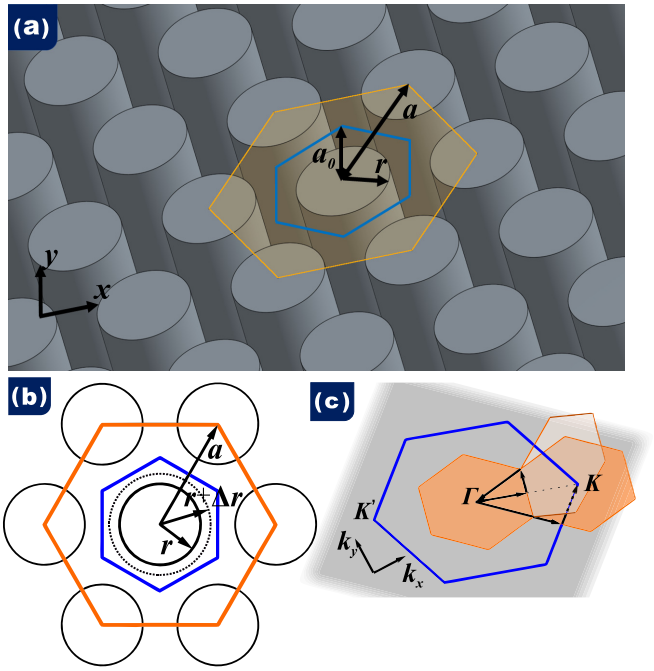

FIG. 1. (a) Structure of the phononic crystal. The rods are periodically arranged with a lattice constant a_0. The conventional unit cell of the triangular lattice is marked by the blue line whereas the expanded unit cell of the triangular lattice is marked by the orange line. (b) Top view of the phononic crystal. r is the radius of the center "atom" whereas $r + \Delta r$ is the modified radius for breaking the translational symmetry. (c) The conventional Brillouin zone and new Brillouin zone correspond to the two different unit cells. The "zone folding" mechanism shows how high symmetry points K and K' are mapped to Γ point in the new Brillouin zone.

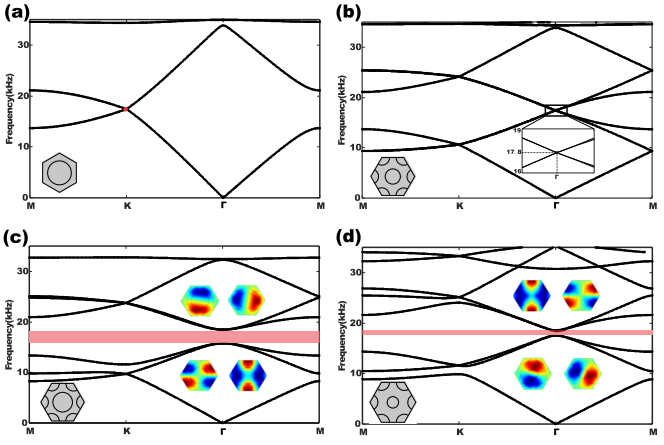

FIG. 2. Band structures for various unit cells. Unit cells are depicted at the bottom left corner in each subfigure. The rods are assumed to be steel and the background medium is air. (a) Original unit cell with a single atom. The single Dirac cone at K is marked by the red dot. (b) Expanded unit cell with double Dirac cones at Γ. (c), (d) Symmetry-broken unit cells with $\Delta r = 1$ mm and $\Delta r = -1$ mm, respectively. Topological band gaps are marked with pink color. p/d eigenmodes are shown with their locations separated by the band gap which indicates the occurrence of band inversion.

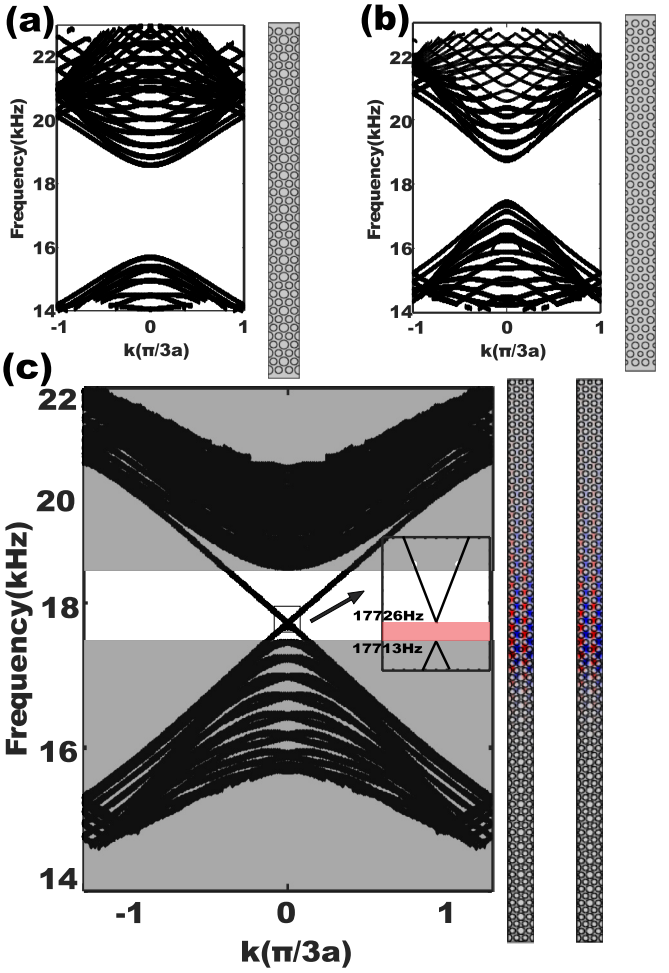

FIG. 3. Band structures of supercells. (a) Band structure of the supercell with $\Delta r = 1.0$ mm. (b) Band structure of the supercell with $\Delta r = -1.0$ mm. (c) Band structures when the two supercells are joined together. One pair of edge states at $f_0 = 17\,800$ Hz (arbitrarily chosen within the edge state frequency band) are shown on the right. The inset figure shows a zoom-in of the minigap.

Further modification of the unit cell is carried out to break the symmetry in order to open a nontrivial topological band gap at the Γ point. In order to do so, the fourfold degeneracy needs to be lifted and separated into two twofold degenerate modes. To this end, we break the translational symmetry T_{a_0} by either increasing or reducing the radius of the center atom while preserving the C_{6v} symmetry. Figure 1(b) shows the case where the center atom radius is modified by Δr. In this study, $\Delta r = \pm 1$ mm. Other values can also be used (Appendix B). As the radius changes, the T_{a_0} symmetry no longer holds and is replaced by T_a corresponding to the new lattice constant a. Figures 2(c) and 2(d) show the opening of the band gap at Γ with $\Delta r = 1$ mm and $\Delta r = -1$ mm. In both cases, two twofold degenerate modes are located on the upper and lower sides of the band gap. Following the convention in quantum mechanics, we can classify these modes to the p_x/p_y and $d_{x^2-y^2}/d_{xy}$ modes according to their eigenmode pressure distributions. In the band structure of the unit cell with $\Delta r = 1$ mm,

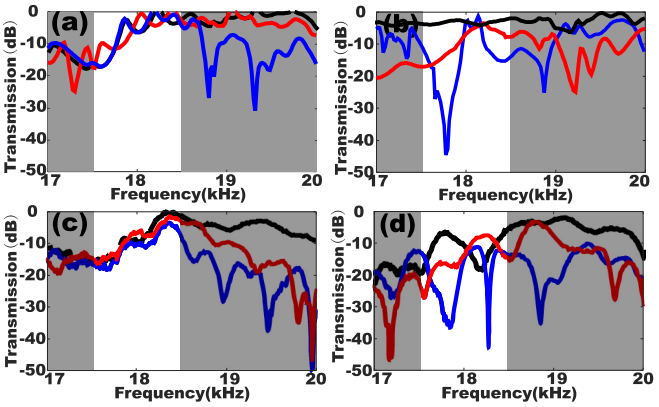

FIG. 4. (a), (b) Simulated transmission spectra with two classes of defects in topological acoustic channels and an ordinary waveguide, respectively. Black curves represent the no defect case, red curves represent the cavity case, and blue curves represent the bending case. (c), (d) Experimental results of the transmission spectra corresponding to (a) and (b), respectively. The topologically protected edge state frequency range is indicated by the light region.

the p_x/p_y modes are located on the upper side of the band gap whereas the $d_{x^2-y^2}/d_{xy}$ modes are located on the lower side. This is exactly the opposite of the band structure of the unit cell with $\Delta r = -1$ mm, which is a necessity to bring about band inversion which occurs when $\Delta r = 0$. The degenerate modes that form the twofold pairs are analyzed by COMSOL MULTIPHYSICS 5.2. The material for the rod is steel with a speed of sound of 6010 m/s and a density of 7800 kg/m^3. The background medium is air, whose speed of sound is 343 m/s and density is 1.21 kg/m^3. It should be pointed out that the material of the rod does not have to be acoustically rigid. This is critical as it provides great flexibility for designing acoustic topological insulators in different background media. The symmetries of these degenerate modes highly resemble those of the p/d orbitals of electrons [25]. Similarly, the spin-1/2 states could be realized through hybridizing the p/d states and further be utilized to form pseudospin states with opposite spin directions. As an analog to the intrinsic spin of electrons in topological insulators, the pseudospin states of acoustic waves are the foundation for building flow-free acoustic topological insulators.

Topological edge states need to be identified in order to achieve robust one-way propagation. Based upon the symmetry-broken unit cells, we design two types of supercells: one with unit cells that have enlarged center atoms ($\Delta r =$ 1 mm) and one with unit cells that have contracted center atoms ($\Delta r = -1$ mm). Bulk band gaps are found in both cases along the horizontal direction of these supercells [Figs. 3(a) and 3(b)]. To investigate the topologically protected edge state, the two supercells are joined vertically and the band structure is shown in Fig. 3(c). The upper supercell has small center atoms while the lower one has large center atoms. The observed edge states from finite element method (FEM) simulations between 17 450 and 18 500 Hz confirm the existence of the two opposite pseudospin states (spin+ and spin−) on the interior boundary between the two supercells. One important feature in the band structure is the existence of a minigap ranging from 17 713 to 17 726 Hz [25], which will be discussed later.

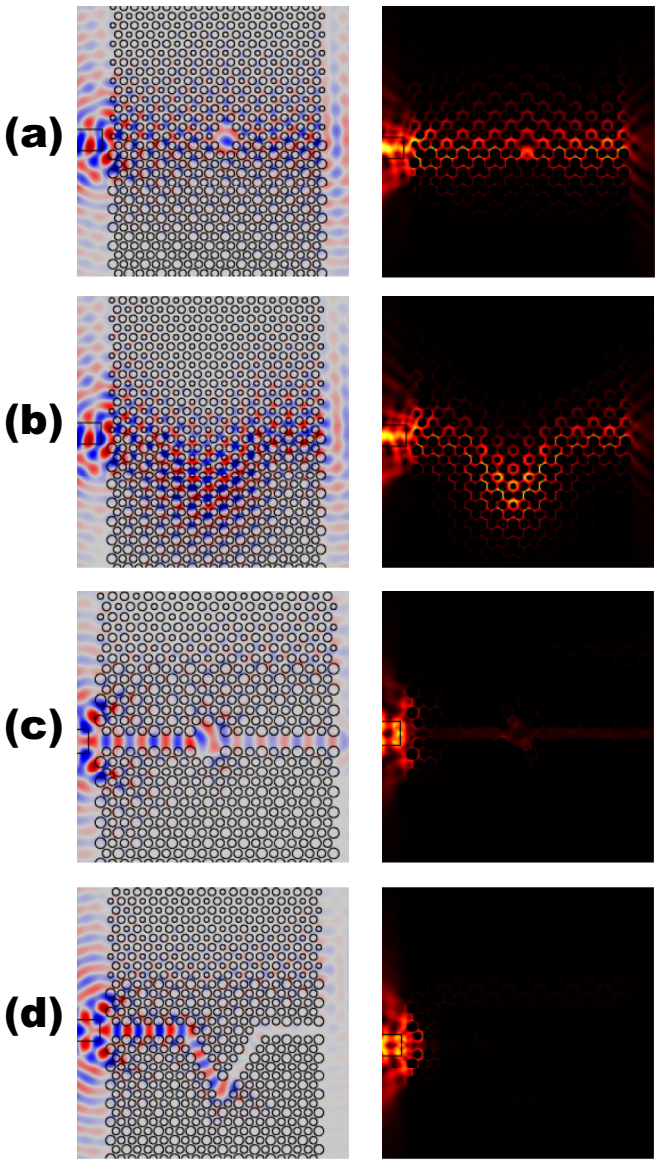

FIG. 5. (a), (b) Acoustic pressure (left) and intensity (right) distributions in the topological insulator with a cavity and a V shape bending. (c), (d) Acoustic pressure and intensity distributions in the ordinary waveguide with the same defects. Considerably lower sound transmissions are observed in the ordinary phononic crystal waveguides. Results are shown at 18 400 Hz.

III. ROBUST ONE-WAY PROPAGATION

The next step is to both numerically and experimentally observe the hallmark of topological insulators, i.e., symmetry protected one-way propagation. To this end, we construct topologically protected channels with non-spin-mixing defects sandwiched by phononic crystals consisting of the two types of unit cells. Non-spin-mixing defects are the ones that preserve the pseudospin states while spin-mixing ones will break the pseudo-time-reversal symmetry and mix the two pseudospin states [25]. A finite-size sound source is placed at the left port of the channel whereas a microphone is located at the exit of the channel. Finite element method simulations are first performed to model the wave propagation through the

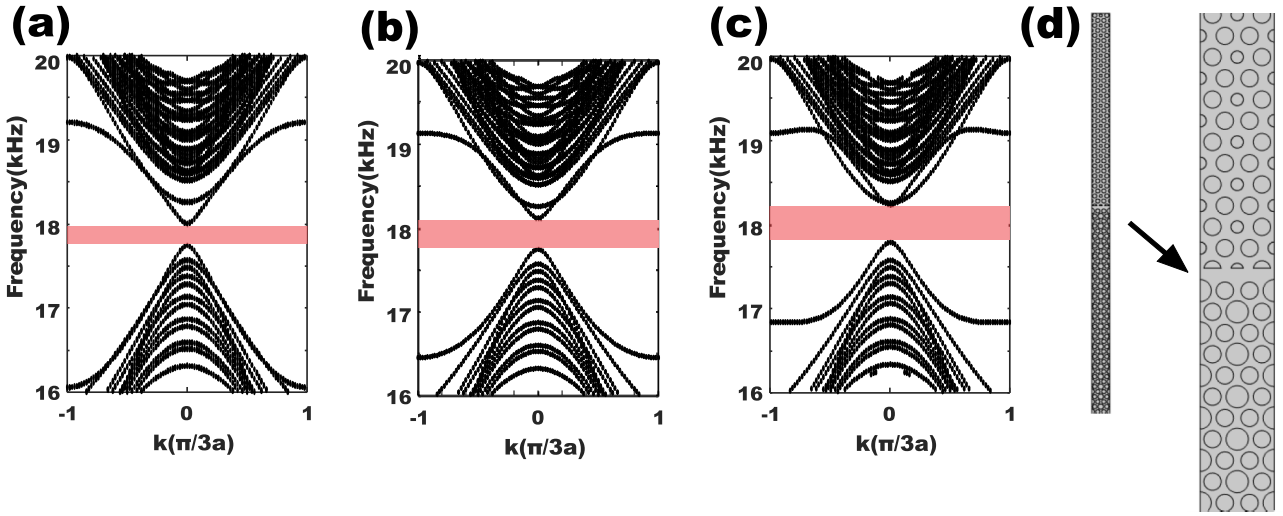

FIG. 6. (a) Simulated band structure of the combined supercell with the cut $d = 4.0$ mm. (b) Simulated band structure of the combined supercell with the cut $d = 3.5$ mm. (c) Simulated band structure of the combined supercell with the cut $d = 3.0$ mm. (d) Supercell figure with the cut $d = 3.0$ mm.

phononic crystal. Three cases defined by the channel topology are studied to showcase the one-way propagation phenomenon, i.e., a straight waveguide without defects, with a cavity, and with a V shape bending. The simulated transmission (the ratio of the acoustic pressure at the exit of the channel to the acoustic pressure at the same point in free space) spectra are shown in Fig. 4(a) and demonstrate no significant sound transmission drops within the predicted edge state frequency band (highlighted by the light region) when defects are present. This can be seen by comparing their results to the ones of the straight waveguide. For comparison purposes, an ordinary waveguide is constructed in the same phononic crystal and wave propagation is simulated with the same input [Fig. 4(b)]. Similarly, we introduce the same sets of defects into the ordinary waveguide. In contrast to the topologically protected channels, the sound transmission spectra here show considerable sound transmission loss in the frequency range of interest, especially for the bending defect case.

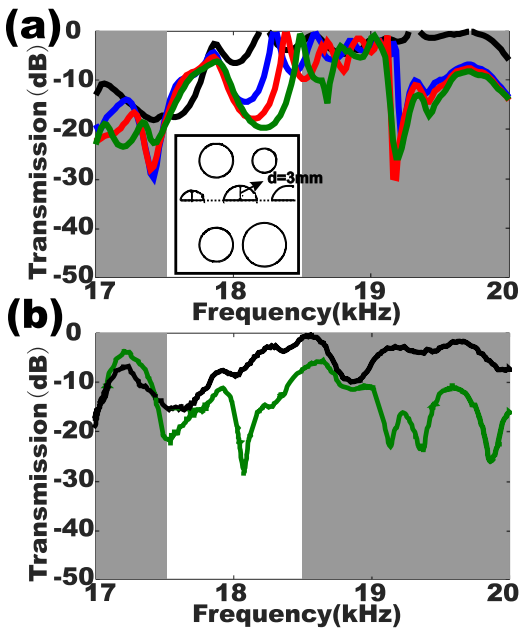

FIG. 7. (a) Simulated transmission spectra of the straight waveguides with different cuts. The black curve represents the case without a cut. The green, red and blue curves represent the cases where d equals 3.0, 3.5, and 4.0 mm, respectively. The cut is shown in the inset figure with $d = 3.0$ mm. (b) The experimental results for the waveguide without a cut (black) and with $d = 3.0$ mm (green).

To validate the simulation, experiments are carried out and the measured sound transmission spectra are shown in Figs. 4(c) and 4(d). Details of the experimental setup can be found in Appendix C. Reasonably good agreement can be observed between the simulation and measurement results, showing the robustness of one-way propagation in the acoustic topological insulator. The discrepancy between the simulation and measurement could stem from the loss in the system, which is not considered in the simulation, as well as fabrication errors and an acoustic source imperfection. The simulated acoustic pressure and intensity distributions at a frequency (18 400 Hz was chosen) within the edge state frequency band show good transmission even with the presence of defects [Figs. 5(a) and 5(b)]. For comparison purposes, the results of ordinary waveguides are shown in Figs. 5(c) and 5(d). As expected, robust one-way propagation cannot be observed.

IV. SPIN-MIXING DEFECTS

Finally, spin-mixing defects are investigated. A pair of pseudospin states are ensured by the pseudo-time-reversal symmetry which relies on the geometric C_{6v} symmetry in the proposed topological insulator. Consequently, the unit cells along the interface between the trivial and nontrivial phases [24] (boundary between the two supercells) which do not fully satisfy the C_{6v} symmetry will slightly mix the two pseudospin states and open a trivial minigap (too small to be visible in the transmission spectra) as shown in Fig. 3. To prove this, we cut through the rods just above the interface to

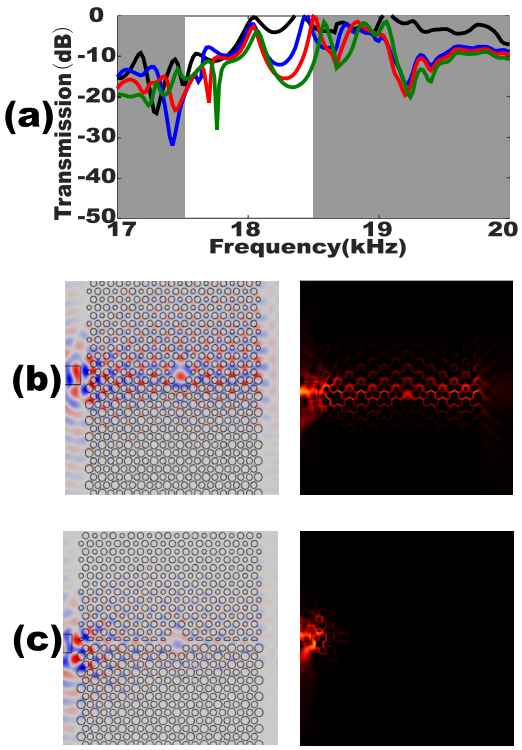

FIG. 8. (a) Transmission spectra of the topological waveguide with a cavity and cut. The black curve represents the case without the cut. Blue, red, and green curves represent the cases with $d = 4.0$, 3.5, and 3.0 mm, respectively. (b) Acoustic pressure and intensity distributions of the topologically protected waveguide with a cavity and no cut. (c) Acoustic pressure and intensity distributions of the case with the same cavity and a cut of $d = 4.0$ mm. Results are simulated at the frequency of 18 400 Hz, chosen to be within the band-gap frequency created by the spin-mixing defect.

introduce significant spin-mixing defects and further break the C_{6v} symmetry. This is done for the straight waveguide case. The extent of the cut is defined as d which varies from 3.0 to 4.0 mm with a step size of 0.5 mm in the simulation [Fig. 7(a)]. The results of band structures (Fig. 6) and transmission spectra [Fig. 7(a)] show that visible band gaps are opened. The width of the band gap seems to be associated with the extent of the cut d which reflects how much the geometric symmetry is broken on the interface. The emergence of the nontrivial band gap is corroborated by the experimental results at $d = 3.0$ mm [Fig. 7(b)]. Similar to the simulation, a clear band gap centered around 18.2 kHz is opened. Note that the edge states can be preserved outside the band gap provided that the cut is not too deep. Finally, it is possible to use the induced band gap for realizing tunable acoustic topological insulators: The intact rods along the boundary can be replaced by the incomplete ones, consequently "switching off" the topological insulator in a frequency band whose bandwidth can be tailored by the extent of the cut. To validate the tunability, a cavity in the straight waveguide is added and the transmission spectra are simulated. The results [Fig. 8(a)] show that the phononic crystal is still robust to the non-spin-mixing defects (a cavity in this case) in the edge state frequency band (approximately from 17.5 to 18 kHz). On the other hand, in the band gap (approximately from 18.0 to 18.5 kHz) created by the spin-mixing defect (cut in this case), the transmission is forbidden. This is verified by acoustic pressure and intensity distributions at 18.4 kHz shown in Figs. 8(b) and 8(c). Note that the width of the band gap can be also tailored by the extent of the cut (size of the spin-mixing defect).

V. CONCLUSION

In conclusion, a flow-free acoustic topological insulator designed based on zone folding is experimentally verified. Robust one-way propagation is observed with the presence of non-spin-mixing defects. The spin-mixing defect is also studied numerically and experimentally, which can give rise to nontrivial band gaps within the edge state frequency band. This finding can help us gain more insights into the physics of pseudospin states as well as on how they can be tailored in topological insulators. It also offers the possibility of tunable acoustic topological insulator devices and may have implications for photonic topological insulators.

ACKNOWLEDGMENTS

The work was jointly supported by the National Basic Research Program of China (Grants No. 2012CB921503, No. 2013CB632904, andNo. 2013CB632702) and the National Nature Science Foundation of China (Grants No. 11134006, No. 11474158, and No. 11404164). M.-H.L. also acknowledges the support of the Natural Science Foundation of Jiangsu Province (BK20140019) and the support from the Academic Program Development of Jiangsu Higher Education (PAPD6).

Y.D. and H.G. contributed equally to this work.

APPENDIX A: UNIT CELLS WITH DIFFERENT FILLING RATIOS

In order to demonstrate that the designed unit cell structure has the ability to obtain double Dirac cones regardless of the

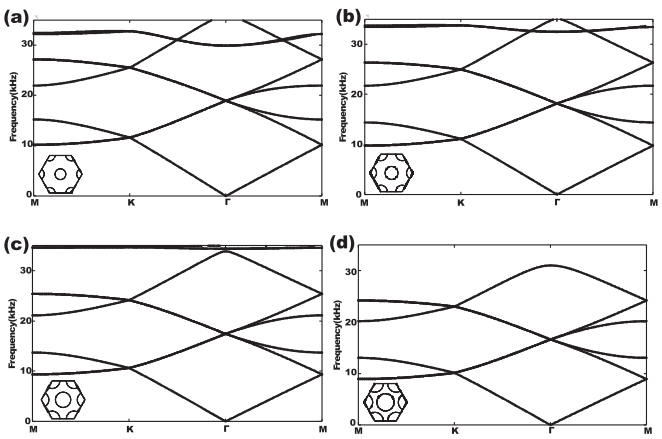

FIG. 9. (a)–(d) Band structures of unit cells with filling ratio 0.25, 0.3, 0.35, and 0.4. Top views of the unit cells are located at the bottom left of each subfigure.

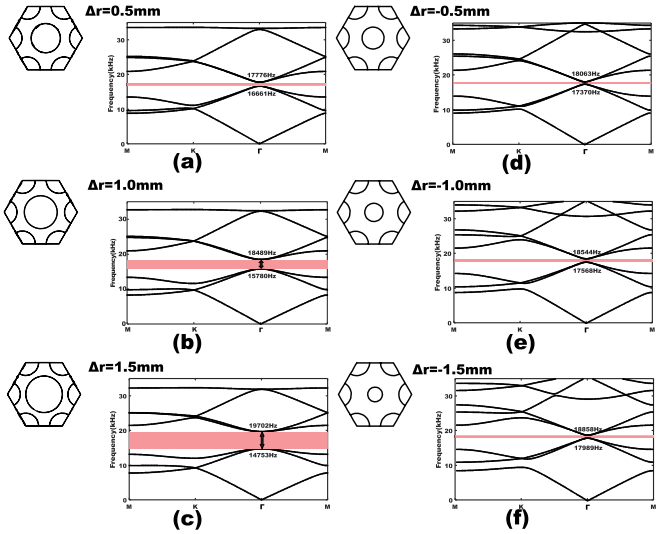

FIG. 10. (a)–(c) Band structures of the expanded unit cells with Δr from 0.5 to 1.5 mm. (d)–(f) Band structures of the expanded unit cells with Δr from -0.5 to -1.5 mm. The band gaps are marked with pink color.

filling ratio of the lattice, unit cells with a filling ratio from 0.25 to 0.4 are simulated with COMSOL MULTIPHYSICS 5.2. The band structures are shown in Figs. 9(a)–9(d). All types of unit cells have double Dirac cones at their Γ point in the Brillouin zones owing to the zone folding mechanism.

APPENDIX B: BAND GAPS WITH DIFFERENT Δr

The band structures of several expanded unit cells with 0.35 filling ratio but different Δr are studied to demonstrate that the band gaps can be opened with different values of Δr. Figure 10 shows the relationship between the width of the band gap and Δr that is applied to the center atom. When Δr is positive, the width of the band gap increases as Δr becomes larger. When Δr is negative, the band gap also increases with the absolute value of Δr, although the change is less significant comparing to the positive Δr case.

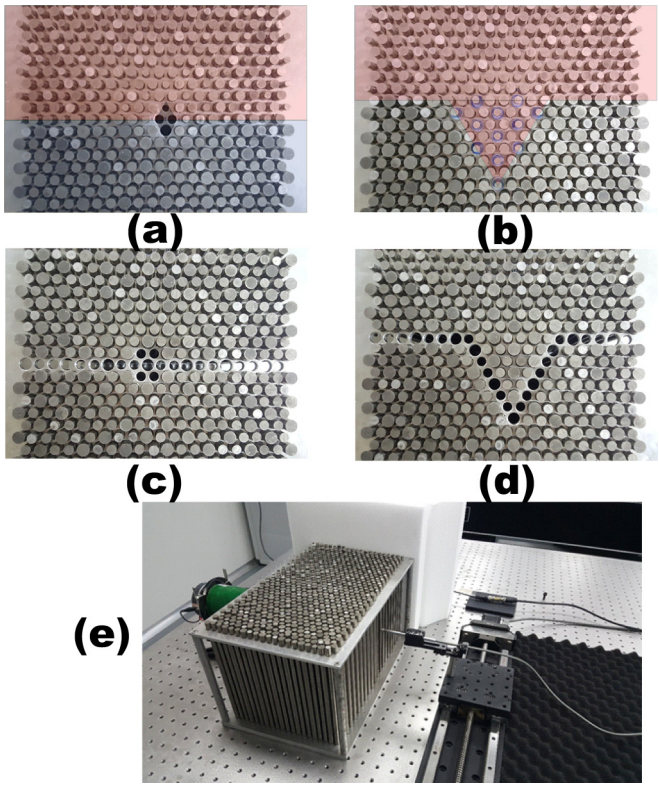

FIG. 11. (a), (b) Acoustic topological insulators structure with defects of cavity and bending. (c), (d) Ordinary waveguide structure with defects of cavity and bending. (e) The experimental system for testing the sound transmission.

APPENDIX C: EXPERIMENTAL SETUP

A detailed setup of the experiment system is shown in Fig. 11. Commercial 304 stainless-steel rods with radii $r =$ 2.5, 3.5, and 4.5 mm are used for constructing the phononic crystal. The heights of these rods are chosen to be 20 cm, nearly ten times the wavelength of sound in air at 17 kHz, to ensure that a two-dimensional approximation is applicable. We placed the large-area transducer near the input port to mimic a plane wave source. A 1/4-in. microphone (B&K type 4939) is placed at the output port to detect the sound wave. The collected signals are acquired and processed by a B&K 3560-C signal analyzer.

[1] R. B. Laughlin, Phys. Rev. Lett. **50**, 1395 (1983).
[2] K. v. Klitzing, G. Dorda, and M. Pepper, Phys. Rev. Lett. **45**, 494 (1980).
[3] B. A. Bernevig, T. L. Hughes, and S. C. Zhang, Science **314**, 1757 (2006).
[4] C. L. Kane and E. J. Mele, Phys. Rev. Lett. **95**, 226801 (2005).
[5] M. Z. Hasan and C. L. Kane, Rev. Mod. Phys. **82**, 3045 (2010).
[6] C. He, X.-C. Sun, X.-P. Liu, M.-H. Lu, Y. Chen, L. Feng, and Y.-F. Chen, Proc. Natl. Acad. Sci. USA **113**, 4924 (2016).
[7] Y. Lumer, Y. Plotnik, M. C. Rechtsman, and M. Segev, Phys. Rev. Lett. **111**, 243905 (2013).
[8] G. Q. Liang and Y. D. Chong, Phys. Rev. Lett. **110**, 203904 (2013).
[9] L.-H. Wu and X. Hu, Phys. Rev. Lett. **114**, 223901 (2015).
[10] A. B. Khanikaev, S. H. Mousavi, W.-K. Tse, M. Kargarian, A. H. MacDonald, and G. Shvets, Nat. Mater. **12**, 233 (2013).
[11] M. C. Rechtsman, J. M. Zeuner, Y. Plotnik, Y. Lumer, D. Podolsky, F. Dreisow, S. Nolte, M. Segev, and A. Szameit, Nature (London) **496**, 196 (2013).
[12] V. Peano, C. Brendel, M. Schmidt, and F. Marquardt, Phys. Rev. X **5**, 031011 (2015).
[13] C. He, Z. Li, X. Ni, X. C. Sun, S. Y. Yu, M. H. Lu, X. P. Liu, and Y. F. Chen, Appl. Phys. Lett. **108**, 031904 (2016).

[14] Q. Wei, Y. Tian, S.-Y. Zuo, Y. Cheng, and X.-J. Liu, Phys. Rev. B **95**, 094305 (2017).
[15] Y.-G. Peng, C.-Z. Qin, D.-G. Zhao, Y.-X. Shen, X.-Y. Xu, M. Bao, H. Jia, and X.-F. Zhu, Nat. Commun. **7**, 13368 (2016).
[16] R. Fleury, A. B. Khanikaev, and A. Alù, Nat. Commun. **7**, 11744 (2016).
[17] A. B. Khanikaev, R. Fleury, S. H. Mousavi, and A. Alù, Nat. Commun. **6**, 8260 (2015).
[18] Z. G. Chen and Y. Wu, Phys. Rev. Appl. **5**, 054021 (2016).
[19] X. Ni, C. He, X. C. Sun, X. P. Liu, M. H. Lu, L. Feng, and Y. F. Chen, New J. Phys. **17**, 053016 (2015).
[20] Z. Yang, F. Gao, X. Shi, X. Lin, Z. Gao, Y. Chong, and B. Zhang, Phys. Rev. Lett. **114**, 114301 (2015).
[21] J. Lu, C. Qiu, S. Xu, Y. Ye, M. Ke, and Z. Liu, Phys. Rev. B **89**, 134302 (2014).
[22] J. Lu, C. Qiu, M. Ke, and Z. Liu, Phys. Rev. Lett. **116**, 093901 (2016).
[23] J. Lu, C. Qiu, L. Ye, X. Fan, M. Ke, F. Zhang, and Z. Liu, Nat. Phys. **13**, 369 (2016).
[24] Z. Zhang, Q. Wei, Y. Cheng, T. Zhang, D. Wu, and X. Liu, Phys. Rev. Lett. **118**, 084303 (2017).
[25] C. He, X. Ni, H. Ge, X.-C. Sun, Y.-B. Chen, M.-H. Lu, X.-P. Liu, and Y.-F. Chen, Nat. Phys. **12**, 1124 (2016).
[26] M. Xiao, W.-J. Chen, W.-Y. He, and C. T. Chan, Nat. Phys. **11**, 920 (2015).
[27] S. Yves, R. Fleury, F. Lemoult, M. Fink, and G. Lerosey, New J. Phys. **19**, 075003 (2017).
[28] R. Süsstrunk and S. D. Huber, Proc. Natl. Acad. Sci. USA **113**, E4767 (2016).
[29] S. H. Mousavi, A. B. Khanikaev, and Z. Wang, Nat. Commun. **6**, 8682 (2015).
[30] R. Susstrunk and S. D. Huber, Science **349**, 47 (2015).
[31] R. K. Pal, M. Schaeffer, and M. Ruzzene, J. Appl. Phys. **119**, 084305 (2016).
[32] C. Brendel, V. Peano, O. J. Painter, and F. Marquardt, arXiv:1701.06330v1.
[33] J. Mei, Z. Chen, and Y. Wu, Sci. Rep. **6**, 32752 (2016).
[34] Y. Li, Y. Wu, and J. Mei, Appl. Phys. Lett. **105**, 014107 (2014).
[35] Z.-G. Chen, X. Ni, Y. Wu, C. He, X.-C. Sun, L.-Y. Zheng, M.-H. Lu, and Y.-F. Chen, Sci. Rep. **4**, 4613 (2014).
[36] F. Gao, Z. Gao, X. Shi, Z. Yang, X. Lin, H. Xu, J. D. Joannopoulos, M. Soljačić, H. Chen, L. Lu, Y. Chong, and B. Zhang, Nat. Commun. **7**, 11619 (2016).